Development of the Mesicopter: A Miniature Autonomous Rotorcraft

Ilan Kroo, Peter Kunz
Stanford University
Stanford, CA

Abstract
This paper describes the development of a centimeter-scale rotorcraft for use as an atmospheric sensor platform. The aerodynamic design of the rotor system is highlighted, while approaches to fabrication, control, and power systems are summarized. 2D Navier-Stokes analysis and design of the rotor sections was combined with 3D nonlinear optimization of the rotors. Results of prototype tests suggest that the concept can be successfully produced and that design methodology is appropriate, despite the insect-like scale of the rotors.

Introduction
This paper deals with a concept that may revolutionize robotic flight vehicles and make possible new kinds of atmospheric science—here and on other planets. The Mesicopter is a tiny, what some would call meso-scale, flight vehicle that flies on its own power and carries sensors for atmospheric research or planetary exploration. Initial devices (see figure 1) range from 1.5 to 5 cm in maximum dimension with a mass of 3 to 15 g. Many interesting scaling issues arise as one shrinks a flight vehicle down to this size. Certain scaling attributes are favorable, such as the increased strength and rigidity of structures at small scales, while others, such as aerodynamics, represent significant challenges.
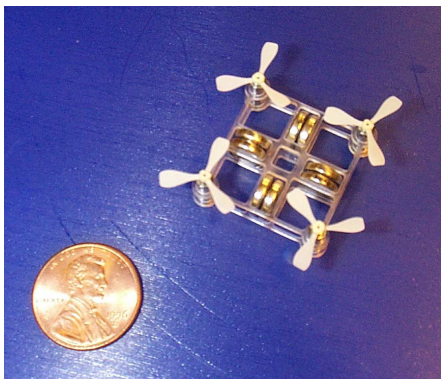
Figure 1. The mesicopter: a meso-scale flying device.

Why a Meso-Scale Flight Vehicle?
A meso-scale flight vehicle is a device that is larger than microscopic, yet much smaller than conventional aircraft, thus the term, *meso*, or in the middle. Interest in flight at this scale is motivated by the revolution in microelectronics and MEMS which will soon permit sophisticated mission-related and flight-control-related sensing with masses in the range of 1g. While realizing that most applications for an aerial robot of this scale are probably a decade or more away, the present investigation addresses some of the fundamental issues with flight at this scale. Such a vehicle would have many unique capabilities including the ability to fly indoors or in swarms to provide sensor information over a wide area at a specific time. The very low mass of these devices might make them attractive for planetary exploration, especially on Mars, due to the high cost of transporting each gram. Although sub-gram imaging systems are not available, miniature aerial robots might be used in the near term for simple atmospheric sensing tasks. If some of the same ideas are applied at a slightly larger scale, several current applications become attractive.

Why a Rotorcraft?
Conventional aircraft require thrust to weight ratios less than 1 because they use a wing to provide lift. In level flight the lift balances the weight and the thrust balances the drag so that the required thrust is the vehicle weight divided by the wing's lift-to-drag ratio. Typical aircraft achieve L/D values from 10 to 20 and thus can fly with considerably less thrust than required by a rotorcraft in hover, for which the thrust produced by the rotor must balance the entire weight. As the scale decreases, however, the ratio of wing lift to drag decreases and so does the conventional aircraft's advantage. In addition, the power required for flight increases with speed, and in some cases at this scale a hovering device requires *less* power than a conventional aircraft.

The power required by a fixed wing aircraft to maintain level flight is:

$$P = TV / \eta_p = W / L/D \ (2W / S\rho C_L)^{1/2} / \eta_p$$

where: T is the thrust, V the forward speed, η_p the propeller efficiency, W the weight, S the wing area, and C_L the wing lift coefficient.

The power required for hover is:

$$P = T \ V_h / M = W \ (W / 2S\rho)^{1/2} / M$$

where: V_h is the induced velocity in hover and M is the rotor figure of merit.

If we compare the power required for hover with that required for level flight of a propeller-powered fixed wing aircraft:

$$P' = (P/W)_{hover} / (P/W)_{fixed}$$
$$= L/D \ \eta_p(W / 2S\rho)^{1/2} / M(2W / S\rho C_L)^{1/2}$$

Now if, just for comparison purposes, we set the disk loading equal to the wing loading and operate the vehicles at the same density:

$$P' = L/D \ (C_L / 4)^{1/2} \ \eta_p/M$$

So rotorcraft start looking more interesting if the L/D and C_L of the fixed wing vehicle are small, as in the case of low Reynolds number flight. If we consider a 15cm span MAV with a L/D of 5 at a C_L of 0.2 (and assume, arguably, that the rotor figure of merit and propeller efficiency are similar), a hovering vehicle would require only 12% more power than the fixed wing device. For larger aircraft this is not at all the case. For a HAE UAV with L/D = 35 and C_L=1.0 the power ratio is 17.5. Of course, the fixed wing MAV flies forward at rather high speeds, while the rotorcraft hovers. This may be an advantage or disadvantage, depending on the intended mission, but the point is that at these scales the often-assumed efficiency disadvantage of rotorcraft is not apparent. As the scale is further reduced, and the L/D and optimal C_L of the fixed wing airplane are further reduced, the comparison is even more favorable. Furthermore, the rotor weight for a given disk area may be significantly lower than that of a similarly-sized wing together with a propeller and tail surfaces.

Rotorcraft may also be desirable for certain missions because of their compact form factor and ability to maintain their position in hover. In many imaging applications, the conventional aircraft's minimum speed limitations are problematic. Current designs for a Mars aircraft indicate that to avoid excessive vehicle dimensions, flight speeds of Mach 0.5 to 0.6 are required, limiting low altitude, high-resolution imaging options. Finally, with a rotorcraft design of this size we can provide sufficient control for a four-rotor vehicle using motor speed control, avoiding problems with control surface aerodynamics and actuation that plague small aircraft of conventional design.

Another alternative to the conventionally-propelled aircraft is a flapping device. Some recent work has suggested that insects exploit the aerodynamics of flapping motion to permit flight at these scales. Although insects may exploit unsteady effects to increase wing maximum lift, and this would allow them to use smaller chord wings, it is not clear that such motion is more efficient than the much simpler rotary wing motion. This investigation of flight at insect scales, therefore began with a miniature rotorcraft

Approach

The development of the Mesicopter started with simple scaling studies to determine if such a concept was at all feasible. This was followed by the development of design methods and manufacturing processes that were needed for Mesicopter fabrication. Based on initial simple scaling models (and nature's overwhelming success in this area) we concluded that flight at these scales is indeed possible, but that building a device to achieve this would not be easy. Major challenges appear in the following areas:

Insect-Scale Aerodynamics: The Reynolds number of Mesicopter rotors lies in the range of 1,000 to 6,000 where aerodynamics are dominated by viscous considerations and few analysis or design tools are available. This is one of the areas in which scaling laws are unfavorable, with lower lift-to-drag ratios and limited rotor lift capabilities. Some of the aerodynamic features are poorly understood in this size regime and means by which improved performance may be realized have been little explored. Because the flow is viscous, some of the simpler tools used for propeller and rotor design are not applicable and basic design rules (e.g. nearly constant inflow) are not appropriate.

3-D Micro-Manufacturing: To achieve high lift-to-drag ratios smooth rotors with 3D surfaces at micro scale dimensions must be built. Traditional micro-fabrication techniques can generate features at and below the desired size scales. Yet the need to produce smooth 3D surface features requires rethinking processing steps commonly used for the building of IC and MEMS structures. Traditional 3D machining methods are not normally employed for the fabrication of parts and devices as thin as 50microns, yet their resolution of a few microns makes them attractive candidates for shaping surfaces within the micron size regime.

Integration of Power and Control Systems: Although many types of batteries with high specific energy are becoming available, identifying very small batteries suitable for the Mesicopter, with good specific energy and high current rates is not easy. The control of these small devices is also a problem. Because of their size, stability time constants are very short and the mass budget for motor/flight control sensors and processing is limited.

Scale Model Development: The basic approach was to develop scalable design and fabrication methods and to start with devices that were larger than the eventual goal. The (super) scale model prototypes are sufficiently large that commercial motors, batteries, and electronics can be employed. The first such prototype is shown in figure 2 with a maximum takeoff weight of about 3g. This device was used to gather data and required an external power supply since the planned Li-Ion batteries were not yet available. The second prototype with a maximum weight of 10-15g is currently being tested and can utilize existing batteries. As these systems are refined, the scale will be reduced to explore the limits of this technology.

Figure 2. Initial prototype

Aerodynamic Design
The operating regime of the meso-scale helicopter poses certain difficulties for aerodynamic analysis and design. Current sizing and motor parameters result in a rotor tip Reynolds number of approximately 5000. Little experimental or computation work has been published on aerodynamic lifting surfaces operating at such low Reynolds numbers (cf. [1]) and it is unclear to what extent classical airfoil and finite wing analysis and design methods are applicable in this flow regime. The highly viscous nature of the flow field, large increases in the boundary layer thickness, and the potential for large regions of separated flow, all

create the potential for large discrepancies in performance from what might be expected based on experience at higher Reynolds numbers (see figure 3). The present approach involves a simplified 3-D rotor analysis and optimization code, coupled with more complete 2-D rotor section analysis. Results from the viscous section analyses are combined with the 3-D design code using regression-based models of the 2-D results. Although this approach is similar to that used for larger scale rotorcraft design, the successful implementation of the approach was not straightforward and some surprising results were obtained.

2-D Analysis Methods: Current computational analysis tools fit into two categories: full viscous flow field solvers working with some formulation of the Navier-Stokes equations, and methods that divide the flow field into an outer inviscid flow region and a viscous boundary layer. We experimented with two Reynolds-Averaged Navier-Stokes solvers including FLO103, developed by our colleague A. Jameson at Stanford [2], and INS2D from NASA Ames [3]. After many test case analyses in this flow regime, the incompressible formulation in INS2D was found to be better suited to analysis at ultra-low Reynolds numbers and was used for the majority of two-dimensional section analysis here.
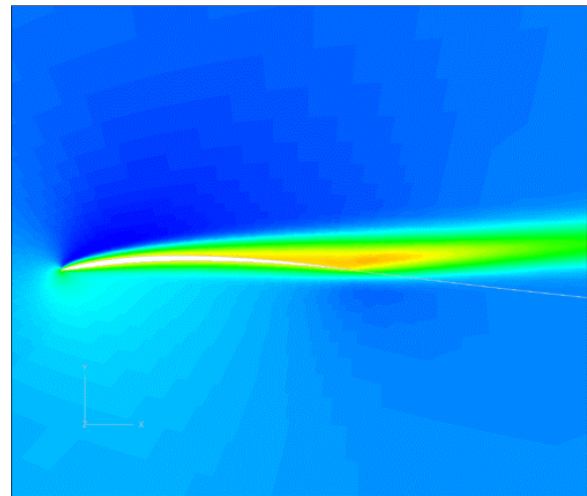
Figure 3. Contours of constant total pressure illustrate the thick boundary layer flow at these conditions. (Re = 5000, α = 8deg)

Programs such as MSES, developed by Mark Drela at MIT [4], couple an inviscid (in this case Euler equation) analysis with an integral boundary layer solver. This code has been used extensively for Mars aircraft studies and appears to give reasonable drag predictions over a narrow range of angle of attack,

but the limitations of the boundary layer formulation become apparent even at angles of attack near the design point.

The programs were compared by analyzing several NACA airfoil sections of varying thickness and camber over a range of Reynolds numbers of interest here. Some results are presented in the following figures, but led us to the conclusion that despite the added complexity and computational effort required for the Navier-Stokes solution, there was a need for the higher fidelity solver. Although the lift and drag of the simpler method agrees well with the Navier-Stokes solution at low lift coefficients, the operational requirements of this very small flight vehicle necessitate maximizing the performance of the airfoil section and the coupled viscous/inviscid solver's limited range of convergence was problematic (figure 4).
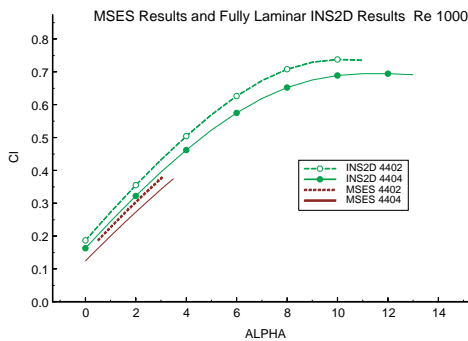
Figure 4. Variation of lift coefficient with angle of attack from INS2D and MSES.

Analysis of many sections was accomplished using INS2D and illustrated the expected sensitivity to Reynolds number, thickness, and camber. A typical result, shown in figure 5, illustrates the importance of low t/c and the very poor section L/D as the Reynolds number decreases below 5000.

The low Reynolds number also limits the maximum lift that can be generated. But here, the effect of Reynolds number below about 10000 is surprising. As seen in figure 6, the maximum lift appears to increase significantly at very low Reynolds numbers.
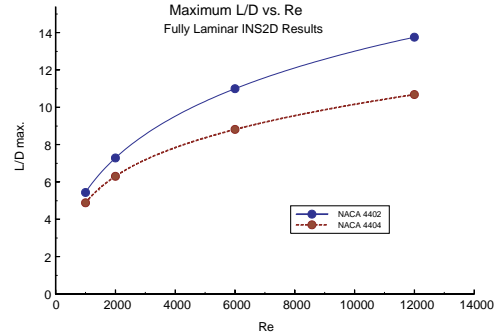
Figure 5. Effect of section t/c and Reynolds number on section L/D.

This is attributed to the fact that the very viscous flow suppresses the formation of high suction peaks near the leading edge and the resulting adverse pressure gradient is reduced. This phenomenon warrants further study, but appears in the experimental data of [5] as well.
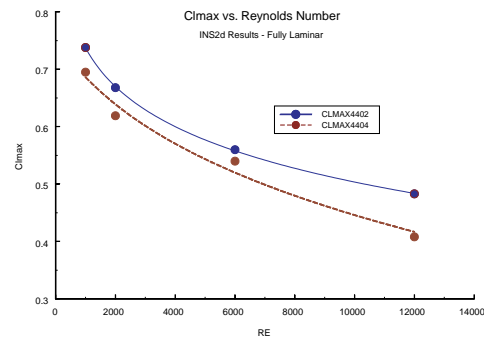
Figure 6. Variation of maximum CL with Reynolds number and thickness.

Since section drag is critical to rotor performance, some effort has been devoted to making sure that the CFD-generated drag values are accurate. Figure 7 illustrates the fine grid around the section nose that is required to obtain reliable drag values. In addition to grid refinement studies, far-field drag methods were used to estimate drag and were found to be a convenient way to produce accurate 2-D drag results.
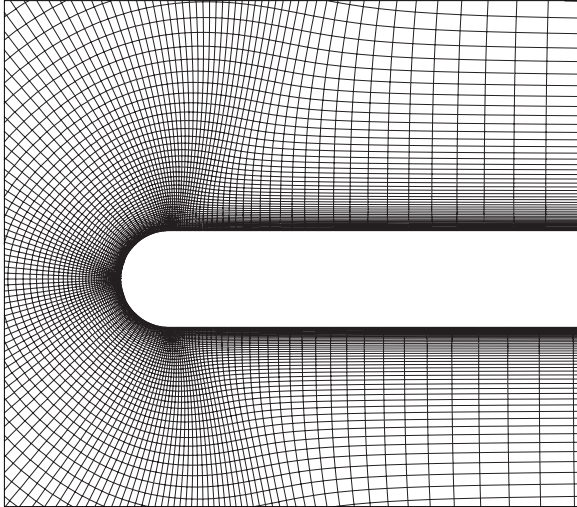
Figure 7. CFD grid around nose of rotor section.

Current work involves additional parametric variation of the camberline and section optimization with explicit manufacturing constraints. As an example of the current study, figure 8 shows the effect of section geometry on drag polars, including NASA sections and more easily manufactured cambered plate geometries.
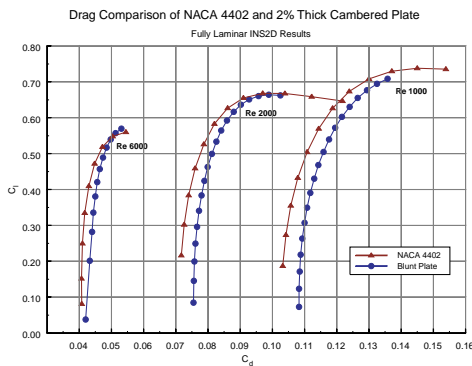
Figure 8. Effect of airfoil geometry on drag polars.

3-D Design: The 3-D rotor design was based on classical blade element methods with inflow computed using momentum and vortex theory. The analysis incorporates viscous effects in several ways, including an estimate of the swirl introduced by blade profile drag. The basic approach is similar to that found in texts such as [6] and so will not be described in detail here. As described in the results section, this simple method was reasonably successful in predicting the rotor performance in hover, but an improved analysis using 3D Navier-Stokes modeling is currently underway.

Since the blade l/d is low and since l/d and C_{lmax} depend strongly on Reynolds number, some of the simpler approaches to design (e.g. minimum induced loss concepts) lead to less than optimal solutions. Nonlinear optimization was therefore employed to determine the blade chord and twist distribution along with rotor diameter and RPM. Models of the section drag polars were constructed from the Navier-Stokes computations and motor performance models, based on tests of the brushless DC motors, were incorporated directly in the optimization.
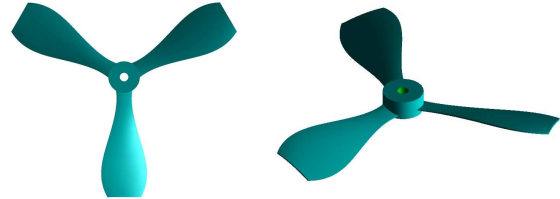
Figure 9. 1.5cm blade geometry determined from numerical optimization.

Optimization results for the larger device show that the rotor is more strongly constrained by maximum solidity. The second prototype requires approximately four times the lift on each rotor and is constrained to 2.2 cm rotor diameter if ungeared commercial DC motors are used. This leads to the geometry shown in figure 10.
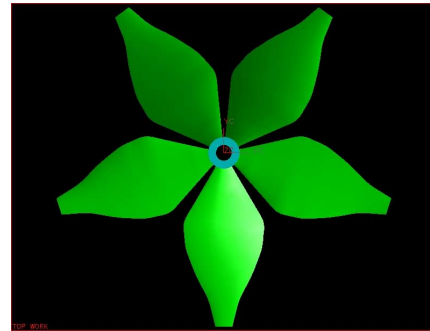
Figure 10. Optimized blade geometry for 2.2 cm rotors.

Rotor Fabrication
One of the more challenging aspects of creating an efficient Mesicopter is the fabrication of the rotor. The optimally designed blades are very thin 3-dimensional structures, with minimum strength and stiffness properties for operation and handling. For the 1.5cm rotors significant aerodynamic performance penalties were predicted for thicknesses in excess of 50 µm. Three material categories were considered -- polymers, metals, and ceramics -- and a variety of manufacturing processes for these material categories were explored. The process selected and

implemented by Stanford's Rapid Prototyping Laboratory is known as Shape Deposition Manufacturing, a sequence of additive and subtractive processing steps for the fabrication of complex 3D parts. Mold SDM is a variation of this process for the creation of complex shaped fugitive wax molds. A spectrum of castable polymer and ceramic materials have been used to make parts from these molds. [7]

The sequence of manufacturing steps is illustrated in figure 11 and involves the following:
● *CAD modeling based on the design parameters:* Chord length, twist angle and cross-section shapes are given at several stations along the radius. Due to the manufacturing and strength considerations, the parts close to the center hub are modified to avoid weak connections and stress concentrations.
● *CNC code generation:* After the model is created, CNC machining code is generated using a commercial CAD/CAM package.
● *Substrate preparation:* Support material is machined to obtain the geometry of bottom surface of rotor by 3-axis CNC mill. (step 1)
● *Polymer casting.* Part material, i.e. polymer, is cast to fill cavity. (step 2)
● *Surface flattening:* Excess polymer on top of the wax surface is removed. (step 3)
● *Material shaping to net shape.* CNC machine geometry of top rotor surface. (step 4)
● *Substrate removal.* If the rotors cannot be pulled out of the substrate directly, wax is melted at 150 degrees C, remaining traces can be removed with BioAct. (step 5)
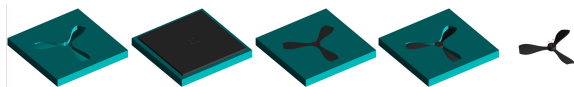
Figure 11. Steps in rotor fabrication

Some of the rotor testing described in the following section revealed that the actual thrust produced was only 80% of that predicted by the aerodynamic analysis. While the aerodynamic approximations made in the interest of reasonable computation times might account for this, it is also possible that the as-built parts did not conform to the intended design. To verify this, detailed studies of the rotor shape were conducted using scanning electron microscopy. An example image of the section shape at 75% of the rotor radius is shown in figure 12.

Figure 12. SEM image of section shape at 0.75R. Chord is approximately 3mm.

In fact, the rotor section shapes did not well approximate the initially designed sections as the desired thicknesses dropped considerably below the minimum 50 µm that could be machined using this process. Subsequent CFD analysis showed that while maintaining small maximum thickness was important to good aerodynamic performance, sections with more uniform thickness distributions were acceptable.

Power Systems
Initial prototypes use commercially available brushless DC motors (made by RMB in Switzerland). These motors achieve very high efficiencies (60%-67%) for their small size (mass as low as 325mg). Of course brushless motors require motor control electronics and to achieve the rated power and efficiency, rather sophisticated closed-loop controllers are required. The motor manufacturer sells a closed loop controller, but this weighs hundreds of grams. For this project, the control electronics have been replicated using small components with a total weight of much less than 1g. A more difficult problem is associated with the voltage requirements for the motors and controllers. Since an input of 4-9 volts is required, a rather large number of cells is necessary to drive the motors, using NiCd or AgO_2 chemistries. Lithium batteries are a natural choice, but small, high current lithiums are not available in the sizes required. Stanford and SRI researchers have explored new lithium polymer technologies that will eventually provide an ideal power source for these devices, but this system is still evolving and is not currently available for the Mesicopter prototypes. A variety of commercial cells have been tested and we constructed a prototype that held 8 small cells (figure 1 and figure 13).

Figure 13. CAD model of multi-cell Mesicopter prototype.

Figure 14. 12g Prototype designed for passive stability.

A more convenient approach involves the use of fewer cells (perhaps as few as 1) and a voltage multiplier to achieve the required voltage levels for the available motors. This is our current approach and electronics development is proceeding in parallel with the system testing.

Control

The basic concept of the 4-rotor design is that vehicle control can be achieved using the motor controllers described in the previous section. This is convenient as it requires no additional electronics and avoids problems associated with additional actuators. By varying the torque applied to the four motors one can achieve roll, pitch, and yaw control, and overall thrust. This strategy for control is not feasible for large rotorcraft, but because of their small size, the Mesicopter rotor inertia is very low and the control bandwidth is high.

Although the basic configuration provides adequate controllability, stability is another issue. A linear model of the rotor aerodynamics was developed and combined with a nonlinear simulation of the vehicle dynamics. This analysis suggested that the vehicle was unstable, but could be stabilized with a moderate amount of rate feedback from a MEMS gyro.

Subsequent studies showed that by carefully positioning the center of gravity and canting the thrustline inward, natural stability might be achieved. A design that incorporates this layout is shown in figure 14. The concept is currently being tested.

The next step in controlling these vehicles involves the development of a communications system for commanding their motion. This system is still in development, but we are working with Intel and other groups on both optical and RF communication options consistent with the very limited mass budget of our current prototypes.

Sensors

Work on performance and stability has remained the focus of this research to date. One of the next areas for study includes possible sensors for improved flight control. An investigation of mission sensors is beyond the scope of the present work. As mentioned previously rate gyros may be used to provide stability augmentation. Very small scale magnetometers and air data systems have been developed for DARPA's MAV program and may be integrated into these devices at some point. Even extremely small scale GPS is a possibility. New concepts for centimeter-level position sensing using carrier-phase differential GPS with a flight system weight of order 1g are currently being considered.

Testing

The testing program to date has included motor, battery, and controller characterization, rotor testing to determine thrust and torque, and complete 4-rotor constrained vehicle tests. Figure 15 shows a single rotor tested on a pivoted arm. This approach has been superceded by more accurate force and moment tests on a test stand constructed for this purpose.
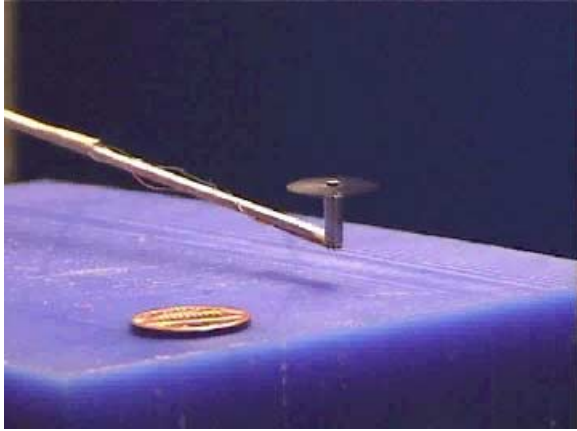
Figure 15. Initial single rotor lift tests.

Figure 16 shows the initial prototype using 3mm motors on a lightweight arm that permitted the device to lift off before stability and control issues were addressed.
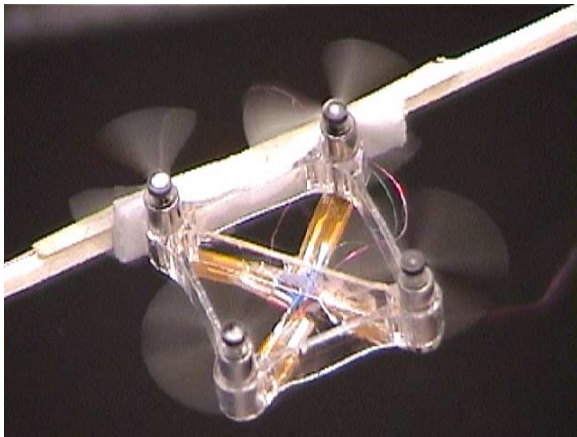
Figure 16. Constrained tests of 4-rotor Mesicopter.

Results of these tests suggested that the aerodynamic design approach was appropriate at this scale, with maximum thrusts of about 80% of the predicted values, despite departures from the assumed section shape. Rotors for the larger prototype have also been fabricated and tested, but show substantially less lift than predicted. This may be related to deflections of the rotor sections under load. Figure 17 shows a large variation in lift during the first tests of the rotor. After additional testing the lift was repeatable at the lower values, suggesting that rotor deformation may be important. Structural analysis is underway and new stiffer materials are being investigated for this version of the device.
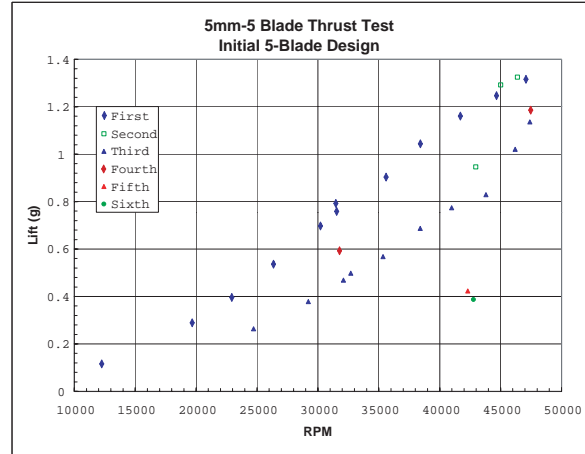
Figure 17. Initial test results for 2.2 cm rotor showing changes in blade geometry.

Conclusions and Future Work

A set of analysis, design, and fabrication methods has been applied to investigate the feasibility of very small rotorcraft. Studies have included a range of vehicle sizes and suggest that Mesicopters as small as 1.5 cm are possible, while devices that can carry 10g of payload may be more easily realized and are of greater current interest. These devices may be used in the near future to carry very simple sensors and may, in the more distant future, be controlled in groups that can provide unique information gathering capabilities.

Continuing work in 3D low Reynolds number aerodynamics will be pursued in parallel with a focused effort on stability, control, and communication. Free flights of our prototypes are imminent. These prototypes will provide an excellent testbed for work on distributed control concepts, aerodynamics, and miniature systems development.

References

1. N. Miki, I Shimoyama, "Analysis of the Flight Performance of Small Magnetic Rotating Wings for Use in Microrobots", Proc. 1998 IEEE International Conf. on Robotics and Automation, Leuven, Belgium, May 1998.

2. Martinelli, L., Jameson, A., "Validation of a Multigrid Method for the Reynolds Averaged Equations," AIAA Paper 88-0414, AIAA 26th Aerospace Sciences Meeting, Reno, NV, January 1988.

3. Rogers, S. E., Kwak, D., "An Upwind Differencing Scheme for the Time Accurate Incompressible Navier-Stokes Equations," AIAA Paper 88-2583, June 1988.

4. Drela, M., Giles, M. B., "ISES - A Two-Dimensional Viscous Aerodynamic Design and Analysis Code," AIAA Paper 87-0424, AIAA 25th Aerospace Sciences Meeting, Reno, NV, January 1987.

5. Thom, A., Swart, P., "The Forces on an Aerofoil at Very Low Speeds," Journal of the Royal Aeronautical Society, Vol. 44, pp. 761-770, 1940.

6. Johnson, W., Helicopter Theory, Princeton University Press, New Jersey, 1980

7. A.G. Cooper, S. Kang, J. W. Kietzman, F. B. Prinz, J. L. Lombardi and L. Weiss, "Automated Fabrication of Complex Molded Parts Using Mold SDM" (PDF, 205k), *Proceedings of the Solid Freeform Fabrication Symposium*, University of Texas at Austin, Austin, Texas, August 1998.